

# ELECTRON PARAMAGNETIC RESONANCE AND ELECTRON NUCLEAR DOUBLE RESONANCE OF CHEMICALLY REACTING TRIPLET STATE SPECIES IN SINGLE ORGANIC CRYSTALS†

CLYDE A. HUTCHISON JR.

*Department of Chemistry and the Enrico Fermi Institute,  
University of Chicago, Ill. 60637, USA*

## ABSTRACT

In this lecture I review a series of both published and unpublished investigations made together with my colleagues and students who are named in *Table 1*. We have studied the organic single crystal system consisting of 1,1-diphenylethylene (DPE) which contained small amounts of diphenyldiazomethane (DPDAM). I describe the ways in which we use electron paramagnetic resonance (EPR), electron nuclear double resonance (ENDOR), optical spectroscopy with polarized light, and x-ray crystallography, to study the photolysis of the DPDAM and the reaction of diphenylmethylene (DPM) with DPE at crystal sites, without serious disruption of the structure of the host crystal. All of the methods and techniques nicely supplement each other to give a detailed picture of this single crystal system. The magnetic resonance methods serve to give a most detailed account of the local structure at the reaction sites in the vicinity of the chemical impurity, DPM.

## 1. INTRODUCTION

Electron paramagnetic resonance (EPR) methods offer many attractive features in connection with the study of chemical reactions in which a paramagnetic species is a reactant or a product. The intensity of EPR absorption may be used to follow the course of the reaction and measure the rate, and to give the actual number of paramagnetic molecules present at any given time. In the case of a reaction in a crystal, a very convenient method of determining the kinetics is thus afforded by EPR and the microwave information carrier offers almost the ideal perturbationless probe. Moreover, if the reactant or product is a relatively dilute triplet state paramagnetic species in a diamagnetic host crystal, the fine structure of the EPR spectrum gives considerable information on the orientation of the species in its crystal environment. In addition, this spectral fine structure gives much information on internal molecular structure and electron spin distribution in the reactant or product. The interactions between the electrons of the paramagnetic molecule and the magnetic nuclei in it offer an additional very powerful means of determining

its geometry, orientation, and spin distribution. Knowledge of such interactions is obtainable in great detail from the hyperfine structure of the EPR spectra and from electron nuclear double resonance (ENDOR) spectra. Furthermore, the so called distant ENDOR spectra, i.e. the ENDOR spectra originating with magnetic nuclei outside a reactive paramagnetic molecule, offer a very important source of information for our purposes of study of chemical reactions in crystals, in that they give detailed knowledge of the structural situation in the environment of a dilute reactive species.

In this lecture I will review a series of studies made by a variety of EPR, ENDOR, optical spectroscopic and x-ray crystallographic methods in our laboratory, at the University of Chicago, which bear on the matters just mentioned, for a particular case. I will be discussing a variety of published and unpublished work<sup>1-9</sup> which is the result of the efforts of quite a number of my colleagues and students. In *Table 1* I summarize their contributions.

*Table 1.* List of contributors to this work

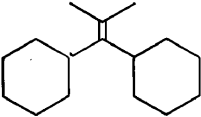
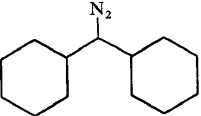
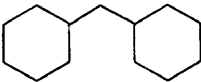
<u>Kinetics</u>	<u>EPR</u>	<u>ENDOR</u>
D. C. Doetschman	R. W. Brandon Professor G. L. Closs C. E. Davoust	B. E. Kohler
<u>X-ray</u>	D. C. Doetschman	<u>Optical</u>
D. C. Doetschman Professor E. Fleischer	B. E. Kohler R. Silbey	Professor G. L. Closs B. E. Kohler

## 2. PRELIMINARY EXPERIMENTS

### 2.1 The molecules

In *Table 2* are listed three molecules with which we will be concerned at the beginning, and their code names which will be used throughout this lecture.

*Table 2.* Molecules

	1,1-diphenylethylene DPE
	diphenyldiazomethane DPDAM
	diphenylmethylene DPM

## 2.2 Some preliminary EPR observations<sup>1,2,6</sup>

When a single crystal of DPE, at a temperature  $\sim 77^\circ\text{K}$ , and containing from 0.0015 to 0.036 mole fraction DPDAM, was irradiated in an EPR spectrometer with the light from a high pressure mercury arc, an intense, very anisotropic, persistent, narrow line (8G width), triplet state spectrum appeared<sup>1,2</sup>. When such a crystal was irradiated at any temperature down to the boiling point of He, we obtained the same results.

When the irradiation was terminated and the crystal was maintained at  $\sim 77^\circ\text{K}$  the EPR signal would remain sensibly constant in intensity for at least several hours. If warmed to  $100^\circ\text{K}$  the signal would decay, exponentially with time, to half the initial intensity in 2 min, and at  $110^\circ\text{K}$  to half initial intensity in 3.5 sec<sup>6</sup>.

When such a DPE crystal containing 0.3 per cent DPDAM was irradiated at  $\sim 96^\circ\text{K}$  with a high pressure mercury arc the initial rate of signal growth gradually decreased until in  $\sim 15$  sec a maximum saturation value would be reached and no further signal increase would occur<sup>6</sup>. If irradiation was then terminated the signal would decay exponentially with a half life,  $\sim 10$  min, or, if the temperature was raised, with a shorter half life as described previously. In either case if the irradiation was begun again at  $96^\circ\text{K}$  or any lower temperature after the decay of the signal, the signal would return.

Our interpretation of such results was as follows<sup>1,2,6</sup>. The long persistence of the triplet state spectrum after termination of irradiation at low temperatures (down to  $< 4.2^\circ\text{K}$ ) was taken to mean that a ground state triplet species was being observed. The very large anisotropy of the EPR spectra, with respect to the direction of  $H_0$ , the laboratory dc field, in the crystallographic axis system, together with the sharpness of the spectral lines, showed clearly that the paramagnetic species was well oriented in the DPE crystal<sup>1,2,4,6,7</sup>. The fine structure of the EPR spectrum was describable within the errors of the measurements by the conventional triplet state spin hamiltonian<sup>5</sup>,

$$\mathcal{H}_s = + |\beta_e| S \cdot \mathbf{g}_e \cdot H_0 + DS_z^2 + E(S_x^2 - S_y^2), S = 1, \quad (1)$$

shown in *Table 3*, with the values<sup>4</sup> of the parameters given in *Table 3*. The magnitude of the value of  $D$  is an expression of the amount of anisotropy of the EPR spectrum. Since the anisotropy arises from the magnetic dipole-dipole interaction<sup>5</sup> which varies inversely as the cube of the distance between the two electrons, the fact that our  $|D|$  is, in this case, about 4 times as large as for a photoexcited triplet state of an aromatic molecule indicated that these two electrons in the triplet state species in DPE spent considerable time together on the same C atom in a pair of orthogonal  $p$  orbitals. In the photoexcited aromatic molecules, considered in the  $\pi$  electron approximation, the Pauli principle keeps the two electrons 1 C-C distance away from each other and this holds down the size of  $D$ .

All of these facts, together with many others, to be discussed subsequently, showed that the DPM molecule with its divalent C atom, often assumed as an intermediate in the photochemical reactions of DPDAM in fluid phase, was responsible for the EPR signals<sup>1</sup>. This divalent C molecule was presumed to

Table 3. Spin hamiltonian parameters at  $\sim 77^\circ\text{K}$ 

(1) $\mathcal{H}_s = +  \beta_e  S \cdot \mathbf{g}_e \cdot \mathbf{H}_0 + S \cdot \mathbf{T} \cdot S = 1$ , for diphenylmethylene	
$D/hc(\text{cm}^{-1})$	+0.39644 (0.00045)
$E_7/hc(\text{cm}^{-1})$	-0.01516 (0.00020)
$g_{zz}$	2.0010 (0.0013)
$g_{xx}$	2.0030 (0.0008)
$g_{yy}$	2.0028 (0.0014)

have been generated by the absorption of light by a DPDAM molecule which had been substitutionally incorporated in the host DPE crystal as it was grown. The absorption of light removed  $\text{N}_2$  leaving the DPM molecule substitutionally incorporated and oriented in the host. The decay of the signal from DPM in dilute crystal solutions, when the irradiation was terminated and the temperature was sufficiently high, was interpreted as the result of chemical reaction with the host DPE to form diamagnetic products. The series of events in which (a) the EPR signal attained a maximum value with continued irradiation, then (b) was removed by chemical reaction of the formed paramagnetic species, and then (c) was regenerated by further irradiation was explained as follows. The growth of the signal was assumed to be terminated by light filtering action of the formed DPM which absorbed all the light necessary for its formation from DPDAM. Warming of the crystal in the dark removed the filter because of the chemical reaction, in the dark, of the DPM with the host crystal, forming products which did not absorb the required light. With the filter removed, further irradiation could generate more DPM. These last suppositions were confirmed by (a) quantitative measurements of all the absorption spectra involved<sup>3,7</sup>; by (b) absolute EPR intensity measurements which showed that the number of divalent C molecules formed at maximum signal intensity corresponded to a small fraction of the number of DPDAM molecules in the light beam and available for DPM production, in the absence of filtering action; and (c) the demonstration that the possible number of signal regenerations was a small finite number, predictable from (a) and (b), which exhausted the supply of DPDAM.

### 2.3 Some preliminary x-ray studies<sup>9</sup>

At the time that the first EPR spectra, which I have just been describing, were obtained, the crystal structure of DPE was unknown. Professor Closs had suggested DPE to us as a suitable host in which we might produce DPM from DPDAM for optical spectroscopic studies. Three reasons for its selection for such purposes were: (1) The probable geometrical similarity of DPE, DPDAM and DPM; (2) the expected chemical inertness of DPE toward divalent C compounds; and (3) the optical transmission of DPE very far into the ultraviolet. Professor Fleischer<sup>9</sup> made some preliminary x-ray diffraction studies of DPE crystals which showed that these crystals had the

properties shown in *Table 4*. These observations, of course, made it possible for us to know the orientations in our EPR spectrometer of our DPE crystals containing DPDAM.

*Table 4.* Preliminary x-ray studies on 1,1-diphenylethylene crystals

---

1.	Orthorhombic
2.	Preliminary space group assignment, <i>Pnc2</i> or <i>Pncm</i>
3.	Unit cell, 2 molecules,
	$a = 19.919/2 \text{ \AA}$
	$b = 7.876 \text{ \AA}$
	$c = 6.759 \text{ \AA}$
4.	2-fold axis along <i>c</i>
5.	Cleavage plane, <i>bc</i>
6.	Optical extinction directions, polarized visible light transmitted normal to cleavage plane, <i>b</i> and <i>c</i>
7.	Polarization direction for visible absorption by DPDAM in DPE, <i>c</i>

---

### 2.4 Some preliminary optical studies<sup>3, 7</sup>

The optical absorptions of polarized light in some DPE crystals containing 0.002 to 0.010 mole fraction DPDAM were studied<sup>3, 7</sup>. The spectra were obtained at 20°K both before and after irradiation with light from a high pressure mercury arc. The results are described in *Figure 1* and in *Figure 2*. The cleavage plane of DPE was known from x-ray studies to be the *bc* plane. The polarization of the DPDAM spectrum along the *c* axis made it possible to know directions in this cleavage plane by visual inspection in DPE crystals containing DPDAM, because they were magenta in colour when viewed against light polarized along *c* and colourless when it was polarized along *b*. The strong polarization of the spectra showed that the guest DPDAM molecules were well oriented. These spectra also showed that DPDAM was disappearing as the paramagnetic species was formed. The amount of paramagnetic species formed was proportional to the amount of DPDAM destroyed. They also explained the termination of growth of EPR signals because of the very intense optical absorptions by the species produced by the photolysis of the DPDAM, which produced the filtering effects mentioned previously.

### 3. EPR EXPERIMENTS<sup>1, 2, 4, 5, 6</sup>

In *Figure 3* are shown the values<sup>6</sup> of the magnetic field strengths at which EPR lines were observed in a light irradiated DPE crystal containing DPDAM, as a function of angle of rotation of the laboratory dc field,  $H_0$ , when the field was rotated in the planes of the orthorhombic DPE crystallographic axis system. (The field strengths are given as proton fluxmeter frequencies.) When  $H_0$  was rotated in the cleavage plane (the *bc* plane) only the three lines of a single triplet state spectrum were observed. When  $H_0$  was rotated in the *ac* plane, only a single spectrum was observed. When  $H_0$  was rotated in the *ab* plane, two magnetically distinguishable molecules were observed. However, the two spectra were only very slightly displaced from each other ( $0.0306\pi(5.5^\circ)$ ). The rotations in the *ab* plane caused  $H_0$  to pass through the principal *x* and *z* axes of the spin hamiltonian (1), within experimental error. The *a* axis bisected the angle between the two *z* axes of the two

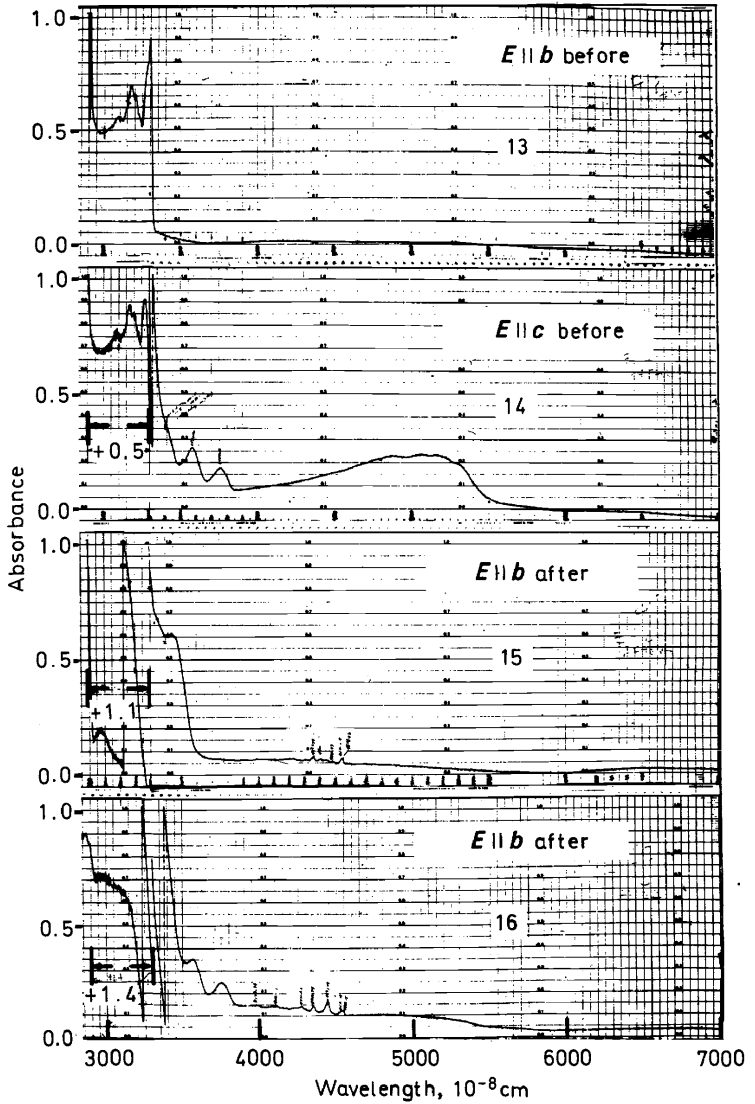


Figure 1. Polarized light optical spectra of 1,1-diphenylethylene (DPE) crystals containing  $\sim 0.002$  mole fraction diphenyldiazomethane (DPDAM) at  $20^\circ\text{K}$ , before and after irradiation with unpolarized light.  $E \times H \parallel a$ .

magnetically distinguishable molecules and the  $b$  axis bisected the angle between the two  $x$  axes. When  $H_0$  was rotated in the other two planes ( $ac$  plane and  $bc$  plane)  $H_0$  passed, within experimental error, through the  $y$  axes (of course, of both molecules, there being only a single spectrum) but missed the  $x$  or  $z$  axes by just a little bit. It thus became very clear that the principal axes,  $x, y, z$ , of the fine structure tensor of (1) were oriented as shown in Figure 4.

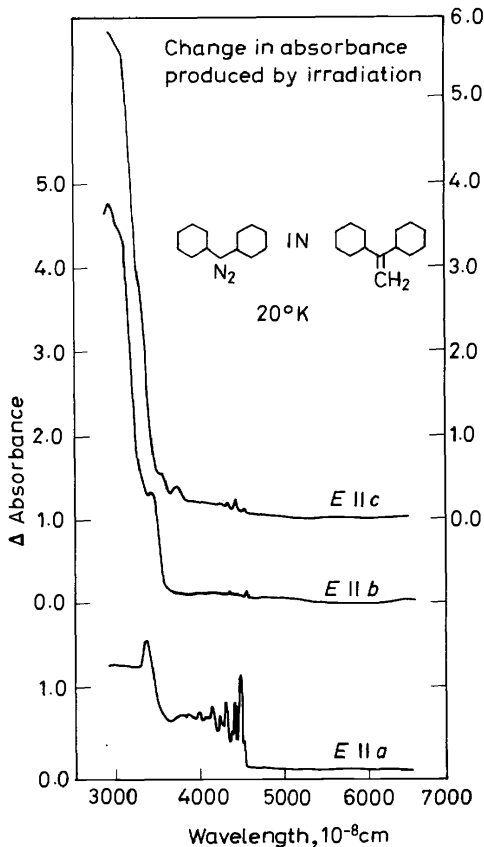


Figure 2. Change produced in the polarized light optical spectrum of 1,1-diphenylethylene (DPE) crystals containing diphenyldiazomethane (DPDAM) by irradiation at 20°K with unpolarized light.

We also noted that the anisotropy of the EPR spectrum was very small for the rotation of  $H_0$  in the cleavage plane ( $bc$  plane) whereas there was an extremely large anisotropy in the other two crystallographic planes. We should now take a look at the DPM molecule<sup>4</sup> described in Figure 5. We believed, for the reasons explained previously, that most of the electron spin density was on the central C atom in an approximately torroidal distribution in two orthogonal  $p$  orbitals. The small anisotropy of the EPR spectrum in the  $bc$  crystallographic plane showed that this  $bc$  plane was in the plane of

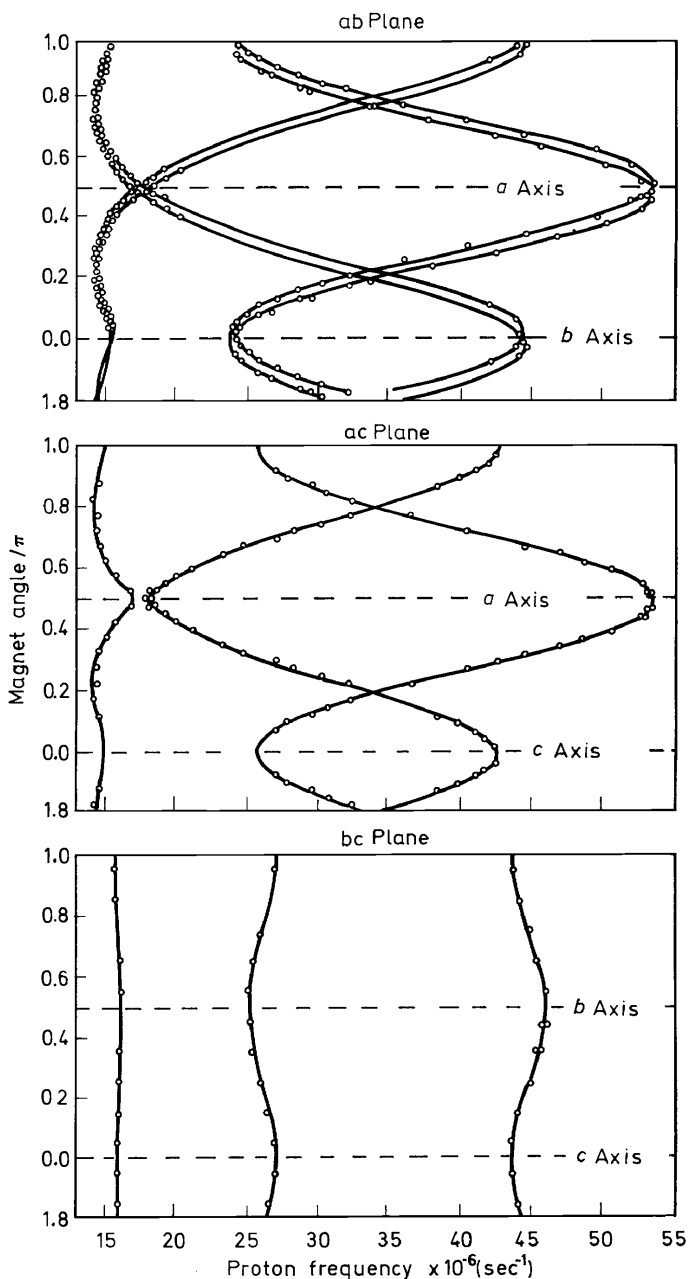


Figure 3. Magnetic field strengths (proton gaussmeter frequencies) for electron magnetic resonance at  $\sim 77^\circ\text{K}$  and at fixed frequency,  $\sim 2.4 \times 10^{10}$  Hz, in single crystals of 1,1-diphenylethylene (DPE) containing diphenyldiazomethane after irradiation with light from Hg-Xe arc. (The circles represent experimental points and the solid lines are calculated using the spin hamiltonian and parameters given in Table 3.)



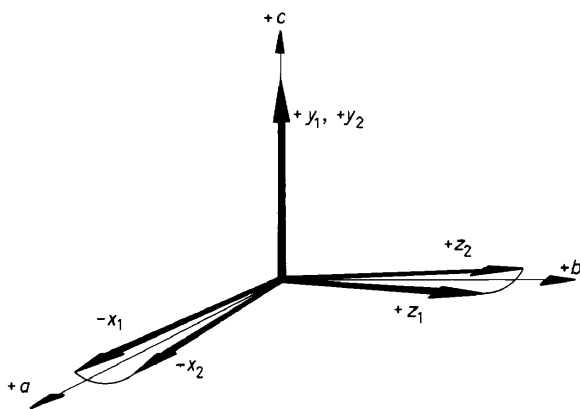


Figure 4. Orientation of the principal axes,  $x, y, z$ , of the fine structure tensor (in the spin hamiltonian, (1), given in Table 3) in the crystallographic,  $a, b, c$ , axis system, for diphenylmethylene (DPM) in 1,1-diphenylethylene (DPE).

the torroidal spin distribution. In fact, if the central  $\overset{2'}{C}-\overset{1}{C}-\overset{2}{C}$  bonding were linear and the two phenyl ring planes were perpendicular to each other, symmetry would demand that  $E$  in the spin hamiltonian, (1), be zero, i.e. that there would be no magnetic anisotropy in the  $xy$  fine structure plane of either of the magnetically distinguishable molecules. Each of the  $p$  orbitals on the central C would be  $\pi$  to one plane and  $\sigma$  to the other. They would give a torroidal spin distribution with axial symmetry. So we pictured<sup>4</sup> the DPM molecule as being a little bent, through angle,  $\theta$ , and a little twisted, through angle,  $\phi - \pi/4$ , from this idealized symmetrical structure which we just mentioned. This distortion introduced the anisotropy in the  $xy$  plane of the molecule. We also saw that the  $y$  fine structure axis, which we found to lie exactly along the  $c$  axis of the crystal for both magnetically distinguishable

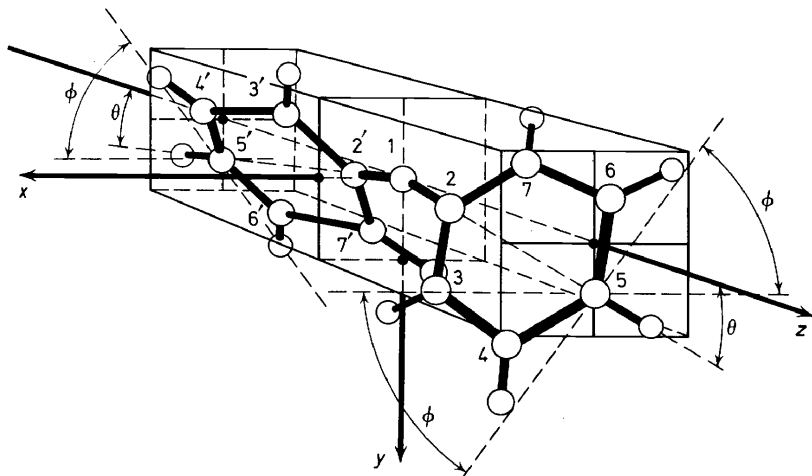


Figure 5. Schematic diagram of the diphenylmethylene (DPM) molecule.

DPM molecules, was therefore a 2-fold axis of the DPM molecule. Thus the molecule was actually describable as a bent and twisted molecule<sup>4</sup> as shown in *Figure 5*, with the 2-fold symmetry axis along the crystal's *c* axis and the molecule's *y* axis. The + value of *D* in the spin hamiltonian, (1), meant an oblate spin distribution with respect to the *z* axis in agreement with our notion concerning its arising from *p* orbitals on the central C atom. The *x* and *z* principal axes of the fine structure tensor were seen to lie in the crystal's *ab* plane, their directions being only very slightly different for the two molecules.

We of course realized<sup>7</sup> at this point what an ideal host the DPE crystal was for polarized light optical studies of the DPM molecule, because of the fact that all molecular axes of all DPM molecules are so nearly coincident in directions.

There was seen to be such a small amount of electron spin on the phenyl rings that their interactions with the protons did not produce a resolvable EPR hyperfine structure. However, substitution of <sup>13</sup>C in the central C position gave large <sup>13</sup>C hyperfine interactions with the triplet state electrons.

Measurements<sup>4</sup> of <sup>13</sup>C hyperfine splitting of each EPR line into two lines afforded a very detailed view of the spin distribution about the central C atom. Both the isotropic and anisotropic components of this tensor interaction, which is described by the spin hamiltonian,

$$\mathcal{H}_C = \mathbf{I} \cdot \mathbf{A} \cdot \mathbf{S}, \quad S = 1, \quad I = \frac{1}{2}. \quad (2)$$

Table 5. <sup>13</sup>C hyperfine interactions of diphenylmethylene (DPM) in 1,1-diphenylethylene (DPE)

(2)	$\mathcal{H}_C = \mathbf{I} \cdot \mathbf{A} \cdot \mathbf{S}$
	$\rho_{2p_x} = 0.565$
	$\rho_{2p_y} = 0.646$
	$\rho_{2s} = 0.0867$

shown in *Table 5*, were measured. If we described the spatial distribution of the electron spin on the central C atom by means of a  $2p_x$  atomic orbital, a  $2p_y$  orbital, and a  $2s$  orbital, the anisotropic components of the <sup>13</sup>C hyperfine interaction gave the spin densities in the *p* orbitals and the isotropic component gave the the spin density in the *s* orbital. The results are given in *Table 5*.

#### 4. ENDOR EXPERIMENTS<sup>4,5,6</sup>

Our most powerful tool for investigating the local structure in the vicinity of a DPM molecule, which had been generated in a DPE crystal, was ENDOR. In the proton ENDOR experiment we determined the nuclear resonance frequencies of the protons in the paramagnetic molecule by sweeping the frequency of an rf field with time. The frequency of this rf field was swept through values in the vicinity of those required for normal proton resonance for the  $|H_0|$  used in the EPR experiment. When proton resonance occurred at the resonance value of the rf frequency, the EPR line intensity changed. This was a very convenient method for measuring proton resonance frequencies in our paramagnetic molecule. The differences between these

proton ENDOR frequencies and the frequency of the EPR lab. magnet's proton gaussmeter, in which the protons occur in diamagnetic water, measured the local magnetic fields which the protons experienced in the paramagnetic molecule, DPM.

As I have already said, the electron spin was mostly on the central C. The rest of it was distributed over 12 C's. The hyperfine interactions of a proton on a C with the electron spin in its vicinity were thus very small. Moreover, with 10 protons, there were  $2^{10}$  lines in the hyperfine pattern of the EPR line for a general direction of  $H_0$ . With so many lines and such small interactions, the result was a single line of 8 G width.

In the case of the ENDOR spectrum, when one watched the EPR intensity as the rf field was swept in frequency, there was just one line for each proton, i.e. for a general orientation of  $H_0$ , 10 lines. Moreover, ENDOR lines were very much narrower than the EPR lines on an energy or frequency scale. The inhomogeneous broadening by local fields, which accounted for a large fraction of the broadening of the lines in these systems, was reduced, on a frequency scale, in the ENDOR spectrum from that in the EPR spectrum by a factor of the ratio of the Bohr magneton to the nuclear magneton. Inasmuch as we scanned frequency and had so many fewer lines than in the unresolved hyperfine pattern of the EPR spectrum, we found<sup>4</sup>, instead of the single 8 G wide line of the EPR spectrum, an ENDOR spectrum of 10 extremely widely spaced, 5 to 10 kHz wide lines as shown in *Figure 6*<sup>4</sup>. The line widths shown in this figure are larger than their true values.  $\sim 5$ –10kHz. for very small modulation fields and sweep rates.

In addition, the signs of the hyperfine interactions were directly observable from the ENDOR spectrum because the oppositely signed interactions displaced the proton ENDOR lines in opposite frequency directions from the gaussmeter frequency, marked G in *Figure 6*. Moreover, if we plotted all the ENDOR shifts versus angle of  $H_0$  in the  $x,y,z$ , axis system of the diphenylmethylene molecule<sup>4</sup>, as in *Figure 7* and in *Figure 8*, the anisotropic component of the hyperfine interaction, combined with our semiquantitative knowledge of the DPM structure and orientation, was sufficient to identify the particular proton of DPM which was responsible for a given ENDOR line. These assignments are given in *Figure 7* and *8* using the numbering system which is used in *Figure 5*.

The interactions of the protons in DPM with the triplet state electrons and with the laboratory dc field,  $H_0$ , were described by the spin hamiltonian,

$$\mathcal{H}_H = -|\beta_n|g_n H_0 \cdot \sum_{k=1}^{10} I_k + S \cdot \sum_{k=1}^{10} \mathbf{A}_k \cdot I_k, S = 1, I_k = \frac{1}{2} \quad (3)$$

( $k$  indexes the protons)

shown in *Table 6*<sup>4</sup>.

The resulting shifts,  $\Delta\nu_k$ , of proton ENDOR frequency of the  $k$ th proton in DPM from the free proton frequency in the same external field were given by this spin hamiltonian. They are also shown in *Table 6*. The expectation values,  $\langle S_x \rangle$ ,  $\langle S_y \rangle$ , and  $\langle S_z \rangle$ , of the electron spin components in the fine structure axis system of *Table 3*, and the direction cosines,  $l$ ,  $m$ , and  $n$ , of  $H_0$ , in the

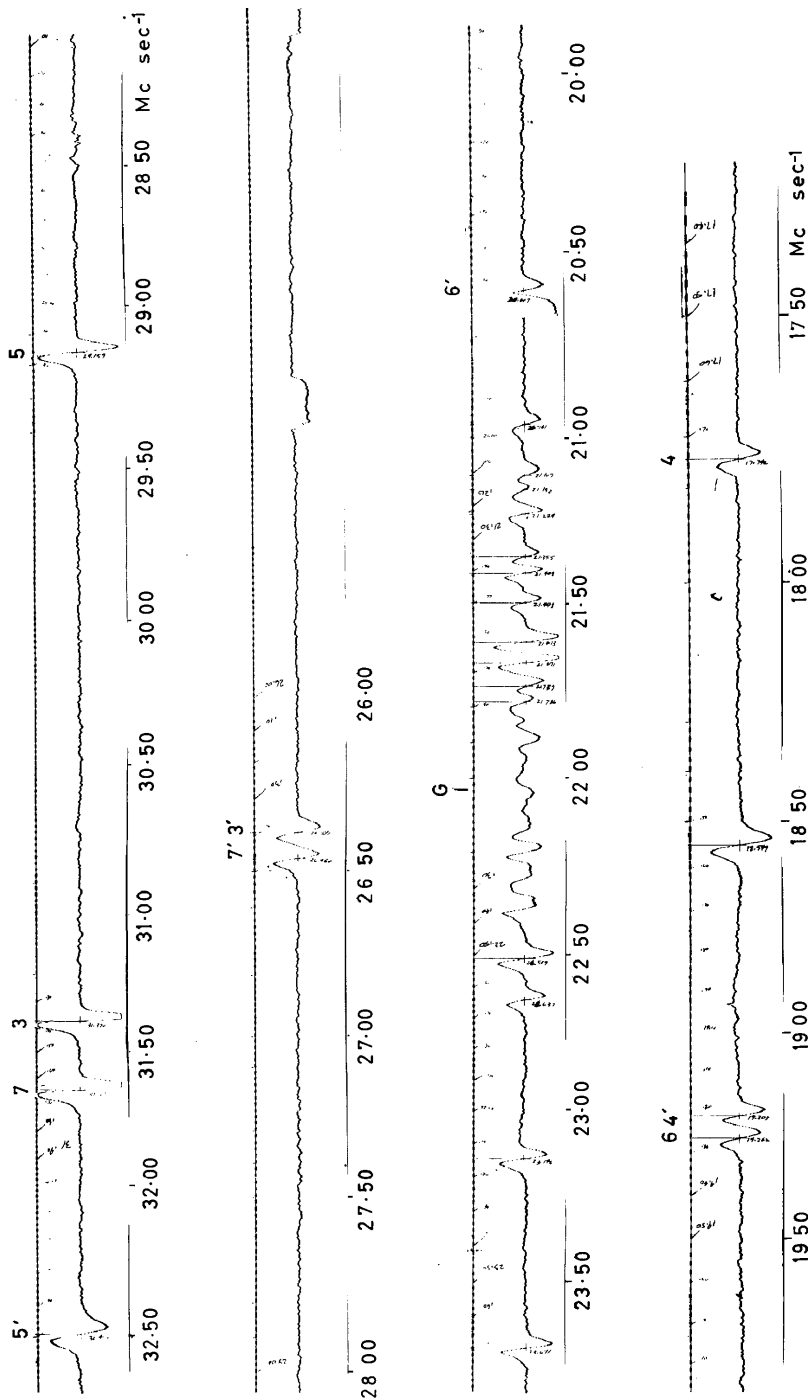


Figure 6. EPR spectrum recording for diphenylmethylene (DPM) in 1,1-diphenylethylene

EPR AND ENDOR OF REACTING TRIPLETS IN ORGANIC CRYSTALS

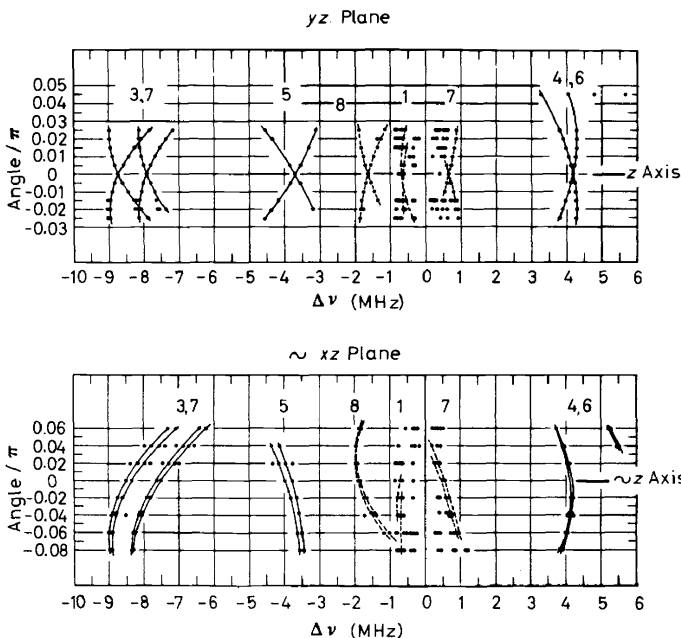


Figure 7. Proton ENDOR shifts vs angle of  $H_0$  for diphenylmethylene (DPM) in 1,1-diphenyl-ethylene (DPE).

same system, were obtained from the EPR data. Then the measured ENDOR shifts of Figures 7 and 8 were fitted with (4) in Table 6 by adjustment of the components,  $A_{rsk}$  of the tensor  $\mathbf{A}_k$ , in (3), for the  $k$ th proton. The resulting values<sup>4</sup> of the  $\mathbf{A}_k$  components are shown in Table 7. These 30 numbers describe the measured interactions of the protons with the triplet state electrons. The precision with which these values are fixed by the experiments is to be noted.

We then considered the model of DPM shown in Figure 5. We fixed<sup>4</sup> the following properties of the model.

- (a) Regular plane hexagon phenyl rings.
- (b) C—C ring bonds  $1.390 \times 10^{-8}$  cm long.
- (c) 1, 2, C—C distance,  $1.425 \times 10^{-8}$  cm.
- (d) C—H bonds,  $1.084 \times 10^{-8}$  cm long, bisecting the hexagon angles.

Table 6. Spin hamiltonian for proton electron hyperfine interaction and proton Zeeman interaction. ENDOR shifts for  $k$ th proton

$$(3) \mathcal{H}_H = -|\beta_n|g_n\mathbf{H}_0 \cdot \sum_{k=1}^{10} \mathbf{I}_k + \mathbf{S} \cdot \sum_{k=1}^{10} \mathbf{A}_k \cdot \mathbf{I}_k$$

$$S = 1, I_k = \frac{1}{2}, k \text{ indexes protons}$$

$$(4) \Delta\nu_k = h^{-1} [ \langle S_x \rangle A_{xxk} + \langle S_y \rangle A_{xyk} + \langle S_z \rangle A_{xzk} - l\nu_p ]^2 + \langle S_x \rangle A_{xyk} + \langle S_y \rangle A_{yyk} + \langle S_z \rangle A_{yzk} - m\nu_p ]^2 + \langle S_x \rangle A_{xzk} + \langle S_y \rangle A_{yzk} + \langle S_z \rangle A_{zzk} - n\nu_p ]^2 ]^{\frac{1}{2}} - \nu_p$$

$\sim xy$  Plane of both molecules

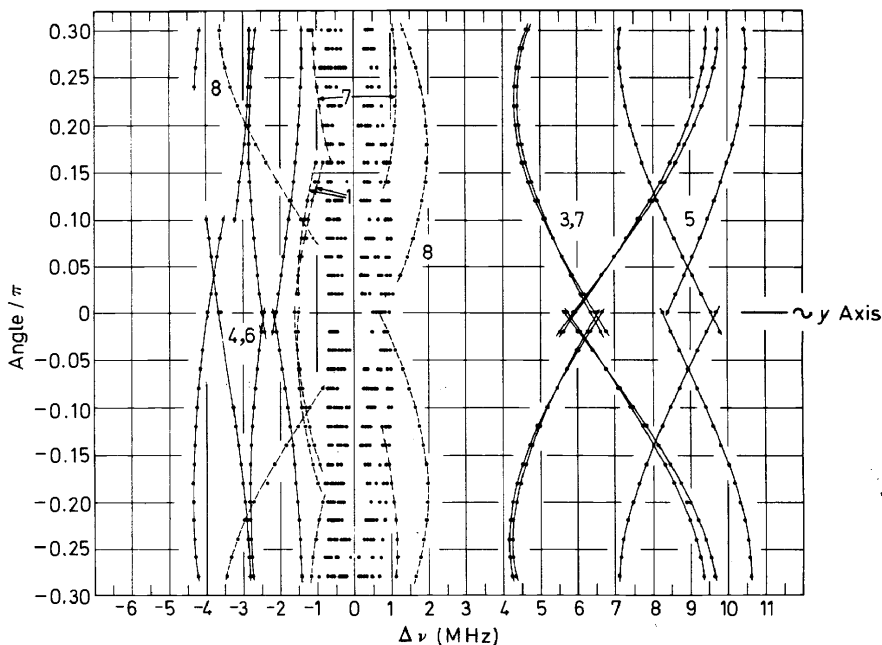


Figure 8. Proton ENDOR shifts vs angle of  $H_0$  for diphenylmethene (DPM) in 1,1-diphenylethylene (DPE).

- (e) Spin distribution on the central C determined by the  $^{13}\text{C}$  EPR data.
- (f) Anisotropic hyperfine interaction components for interaction of the proton with electron spin on adjacent C, value given by previous measurements on photoexcited aromatic molecules in triplet states.
- (g) Spin distribution on ring C's not adjacent to  $k$ th proton, 2 point spins, 0.7665 Å above and below the hexagon plane.

Table 7. Best values of the element of the  $A_k$  for diphenylmethene in 1,1'-diphenylethylene (DPE). (Standard deviations are given in parentheses.)

Proton Position $k$	3	4	5	6	7
$A_{xxk}/h$ (MHz)	-7.6336 (0.0042)	+2.0808 (0.0072)	-9.4227 (0.0031)	+3.5157 (0.0065)	-7.9418 (0.0036)
$A_{yyk}/h$ (MHz)	-6.5061 (0.0212)	+2.5141 (0.0025)	-9.9857 (0.0087)	+4.1849 (0.0022)	-6.5422 (0.0169)
$A_{zz}/h$ (MHz)	-7.9720 (0.0031)	+4.1687 (0.0013)	-3.8070 (0.0026)	+5.8278 (0.0034)	-8.7763 (0.0023)
$A_{xyk}/h$ (MHz)	+2.8889 (0.0070)	+0.6828 (0.0024)	-2.1519 (0.0031)	+0.7412 (0.0020)	+3.1182 (0.0056)
$A_{xzk}/h$ (MHz)	-1.4376 (0.0109)	-0.0706 (0.0043)	+0.9089 (0.0105)	+0.0020 (0.0078)	-1.1519 (0.0083)
$A_{yzk}/h$ (MHz)	-0.9560 (0.0146)	+0.4939 (0.0036)	+1.9088 (0.0158)	+0.5535 (0.0036)	-1.1587 (0.0107)

We allowed the following properties to vary:

( $\alpha$ ) Angle of bend,  $\theta$ .

( $\beta$ ) Angle of twist,  $\phi$ .

( $\gamma$ ) 7 distinguishable spin densities,  $\rho_i$ , on the C atoms, C = 1 to 7.

For a given value of the pair,  $\theta$ ,  $\phi$ , we adjusted the 7  $\rho_i$  to give a best fit. We did this for numerous  $\theta$ ,  $\phi$ , pairs in the range  $0.060\pi \leq \theta \leq 0.110\pi$ ,  $0.250\pi \leq \phi \leq 0.400\pi$ . The best fit gave us the values of  $\theta$  and  $\phi$  and the spin densities. The spin density values are given in Table 8. The angle values will be given in a subsequent table.

Table 8. Best values of spin densities of diphenylethylene in 1,1'-diphenylethylene (DPE) and their standard deviations  $\sigma$

<i>i</i>	1	2	3	4	5	6	7	Total
$\rho_i$	+0.590	-0.022	+0.101	-0.0392	+0.1108	-0.0381	+0.1215	1.060
$\sigma\{\rho_i\}$	0.062	0.037	0.012	0.0051	0.0044	0.0043	0.0090	

If we now look again at Figures 7 and 8, we see that there are many ENDOR lines not assignable to protons in the DPM molecule. These lines were very important<sup>6</sup> for our purposes. They originate with the protons of the DPE host crystal molecules. Some of these lines, which come from protons of DPE which are relatively close to the DPM molecule, show relatively large anisotropies of ENDOR shift,  $\Delta\nu$ . There are many from greater distances which lie very near the proton gaussmeter frequency and have  $\Delta\nu \cong 0$ . Six of these plots of ENDOR shift versus angle of  $H_0$  were fitted<sup>6</sup> by least squares adjustment of values of components of  $\mathbf{A}_k$ , in the same manner as we have described for the proton in the DPM molecule. Values of these components are given in Table 9<sup>6</sup>. Values of the isotropic parts,  $^1A_k$ , of these tensors are given in the last row of this table. Only half the tensors are given since, because

Table 9. Best values of the elements of the  $\mathbf{A}_k$  and the values of  $^1A_k$  of 1,1-diphenylethylene protons near diphenylmethylenes in crystals of 1,1-diphenylethylene. (Standard deviations are given in parentheses.)

Proton Position <i>k</i>	1(0, 0, 1)	7(0, $-\frac{1}{2}$ , $-\frac{1}{2}$ )	8(0, $-\frac{1}{2}$ , $-\frac{1}{2}$ )
$A_{xxk}/h$ (MHz)	-1.172 (0.039)	+0.115 (0.016)	+1.998 (0.014)
$A_{xyk}/h$ (MHz)	+0.180 (0.007)	+1.251 (0.006)	+2.724 (0.006)
$A_{xzk}/h$ (MHz)	-0.102 (0.032)	+0.787 (0.020)	+1.011 (0.010)
$A_{yyk}/h$ (MHz)	+1.790 (0.005)	-0.396 (0.008)	-0.344 (0.006)
$A_{yzk}/h$ (MHz)	+0.175 (0.009)	+0.673 (0.014)	+0.701 (0.012)
$A_{zzk}/h$ (MHz)	-0.661 (0.003)	+0.627 (0.004)	-1.694 (0.003)
$^1A_k/h$ (MHz)	-0.014 (0.013)	+0.115 (0.006)	-0.013 (0.005)

of the 2-fold axis, the others are different from the given ones only with respect to algebraic signs of the values. It is to be noted that the isotropic components, which measure the electron nucleus contact interaction, have values larger than their standard deviation and thus we see that there is actually a small amount of triplet electron spin on the host DPE molecules.

Having arrived at  $\mathbf{A}_k$  values for host DPE proton interactions with electron spin on DPM molecules, we extracted the values of the anisotropic parts of these interactions, which arose from magnetic dipole-dipole interactions between DPE protons and electron spin on DPM. These anisotropic interactions depended on the positions,  $r_k$ , of the DPE protons, the positions,  $r_i$ , of the point electron spins in our DPM model, and the spin density  $\rho_i$ , at each C of the DPM. We used the values of  $\rho_i$  and  $r_i$  given previously, as determined by ENDOR, and adjusted the  $r_k$  to give a least squares best fit to the  $\mathbf{A}_k$ . In Table 10<sup>6</sup> are given the values of the  $r_k$  components, for DPE protons, in the DPM  $x, y, z$ , axis system with the origin fixed at the central C of DPM.

Table 10. Coordinates of 1,1-diphenylethylene protons near diphenylmethylene molecules in 1,1-diphenylethylene crystals. (Standard deviations are given in parentheses.)

Proton Position $k$	1,(0, 0, 1)	7,(0, $-\frac{1}{2}$ , $-\frac{1}{2}$ )	8,(0, $-\frac{1}{2}$ , $-\frac{1}{2}$ )
$x$ (Å)	+0.163 (0.053)	-1.838 (0.025)	-2.495 (0.005)
$y$ (Å)	+4.100 (0.044)	-0.623 (0.020)	-1.707 (0.006)
$z$ (Å)	+0.382 (0.072)	+3.874 (0.013)	+0.578 (0.010)

Before proceeding with an assignment of these proton positions to particular protons of particular DPE molecules, we must further consider the optical spectroscopic and x-ray diffraction studies.

## 5. OPTICAL EXPERIMENTS<sup>3, 7</sup>

As I mentioned before, the DPE crystal was an excellent host for the study of the polarized light, optical absorptions by DPM molecules because they were held in this crystal with  $x, y$ , and  $z$  axes of all four molecules per unit cell nearly parallel or anti-parallel.

The most striking feature<sup>3, 7</sup> of the visible ( $\sim 4500$  Å) spectrum of the DPM molecule, at both  $\sim 20^\circ\text{K}$  and  $\sim 77^\circ\text{K}$ , was a structured absorption band of medium intensity ( $f \sim 0.2$ ) which appeared only in polarization along the crystallographic  $a$  axis. All structure is accounted for by assuming a 0—0 transition at  $22174\text{ cm}^{-1}$  and vibronic additions of 192, 520 and  $956\text{ cm}^{-1}$ . For  $b$  and  $c$  axis polarization there was an absorption band of approximately  $\frac{1}{10}$  the intensity of the  $a$  polarized band. This band had its origin at  $22022\text{ cm}^{-1}$ . It was sensibly the same in intensity and position for all polarization directions in the  $bc$  plane but there were small differences at shorter wavelengths for the  $b$  polarized and the  $c$  polarized spectra.



Careful analysis showed that the *a* polarized band and the *bc* polarized band were actually different electronic transitions and not the same transition with electronically forbidden, vibronically allowed components in one of the orientations of the polarization.

It was very clear<sup>3,7</sup>, before the availability of ENDOR data, that the optical spectrum showed that the optically absorbing species generated by the irradiation of DPE crystals containing DPDAM was cylindrically symmetrical with respect to electric dipole absorption. The optical information thus showed that if this species were the DPM molecule of *Table 2* and *Figure 5*, its geometry might be expected to approximate the situation in which the 5',2'-1-2,5 C's lay in a straight line near the *a* axis and the planes of the two phenyl rings were more nearly normal to each other than parallel to each other.

We made relatively simple calculations of the energies of the possible electronic states of a DPM molecule which resulted from assigning the 14 electrons ( $\pi$  electrons of phenyl rings and 2 electrons on the divalent C) to Hückel orbitals of lowest energy, assigning spins, taking properly antisymmetrized products of these spin orbitals and introducing electron repulsion in a manner similar to that of Longuet-Higgins and Pople<sup>29</sup> for free radicals. The approximation of neglect of differential overlap was employed<sup>30</sup>. The calculated electric dipole transitions for such a model with the phenyl rings parallel (i.e.,  $\phi = 0$ ,  $\theta = 0$ , in *Figure 5*) are in disagreement with experiment for the *xy* polarizations as far as relative frequencies and positions are concerned, as expected. Such calculations for a DPM molecule with phenyl rings perpendicular (i.e.  $\phi = \pi/4$ ,  $\theta = 0$  in *Figure 5*) gave much better agreement. The small disagreements that remained may be interpreted in terms of a small bend by angle,  $\theta$ , and a small change in  $\phi$ , from that just mentioned, by means of more accurate configuration interaction calculations which are currently in progress.

There was thus seen to be a striking consistency between the results of EPR, ENDOR and optical absorption investigations of the DPM molecule oriented in the DPE crystal host, with respect to the conformation of the divalent C molecule and to its angles of orientation in the DPE structure.

## 6. X-RAY STUDIES<sup>6, 8, 9</sup>

As I stated earlier in this lecture. the x-ray diffraction patterns of the DPE crystal were consistent only with space groups *Pnc2* or *Pncm*. The density of the crystal showed that there must be two molecules per unit cell. Thus *Pncm* required *2/m* symmetry for the molecule, DPE, and was rejected. A consideration of the *Pnc2* revealed that when packing energies and proton-proton internuclear distances were computed, any arrangement corresponding to this space group was impossible. The conclusion was therefore reached that some type of disordering existed in these crystals.

We knew that the DPM molecules were well oriented in the DPE crystals and that there were only two magnetically distinguishable molecules. We knew that the symmetry of the host crystal determines the orientation of the guest molecules. Thus whatever the disordering was, it must preserve the observed orientation of both the EPR fine structure and ENDOR hyperfine

structure principal axis systems of the substitutionally incorporated DPM molecules. Therefore we considered a disordering in which different domains are translationally coherent with cell edges exactly parallel or antiparallel. The basic domains were required to have a structure which, when averaged over all domains, gave  $Pnc2$  or  $Pncm$ . A space group was sought which

- (a) was a subgroup of  $Pnc2$  or  $Pncm$ ;
- (b) would allow the long axis of DPE to be nearly parallel to the  $a$  axis (EPR of DPM); and
- (c) would have a 2-fold axis at molecule sites which were along the  $c$  axis.

$Pnca$  satisfied these requirements.  $Pnca$  comes from  $Pncm$  by removing the mirror in the  $ab$  plane and by expanding the  $a$  length to twice the value which I gave in Table 4. The structure of DPE was thus one in which the domains have space group symmetry,  $Pnca$ , the  $a$  length is 19.918 Å, there are four molecules per unit cell, two of the molecules are related to the other two by an inversion (which cannot be detected by EPR of DPM oriented in DPE), there is a 2-fold axis along the  $c$  axis at each molecule site, the long axes of the DPE molecules lie only slightly off from being parallel to the  $a$  axis, and the disordering is such that crystallographic axes of all the domains are

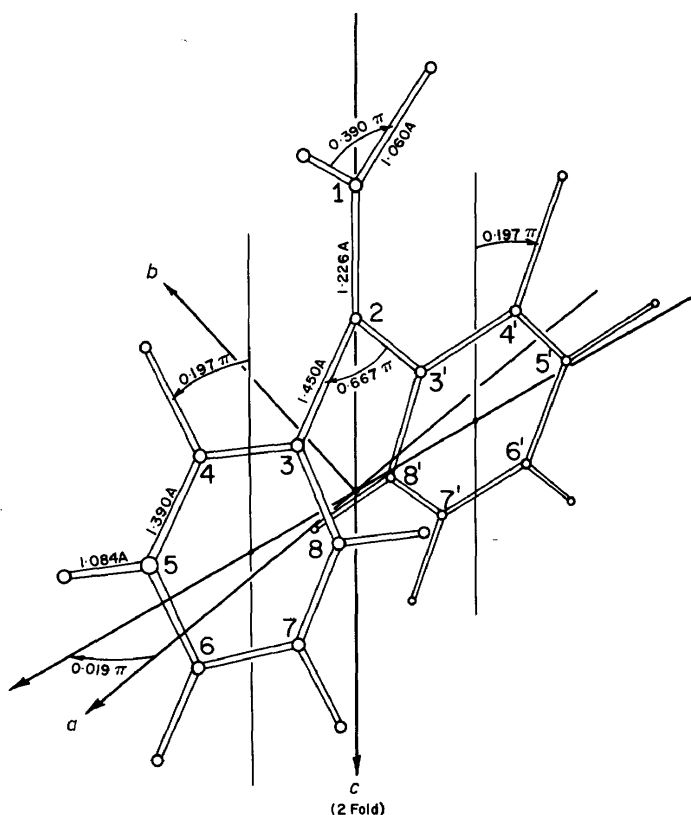


Figure 9. Simplified model of the 1,1-diphenylethylene (DPE) molecule.

parallel or antiparallel and translational coherence exists between domains such that there is equal probability that any unit cell be displaced along  $a$  by either  $na$  or  $(n + \frac{1}{2})a$ ,  $n$  any integer.

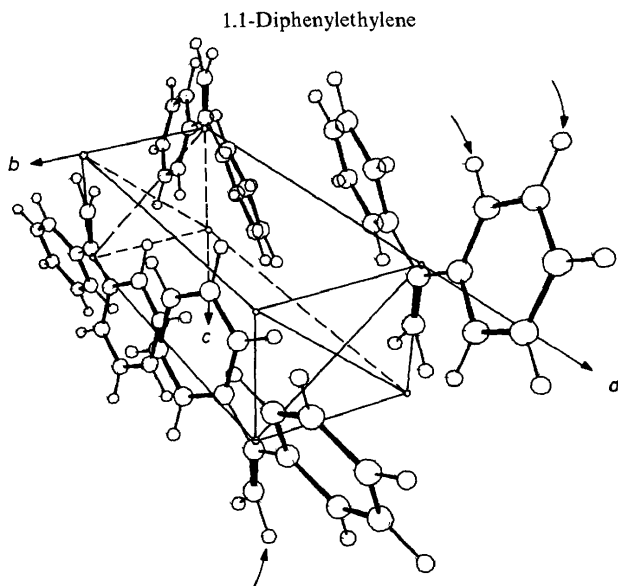


Figure 10. View of the 1,1-diphenylethylene (DPE) crystal structure.

We used the values of the C atom coordinates determined by x-ray diffraction for the construction of a model of the DPE molecule which is shown in Figure 9. In this DPE model, the phenyl rings were taken to be planar regular hexagons lying in the planes which gave the best fit to the ring C atom coordinates determined by x-rays. Each ring edge was taken to be 1.390 Å.

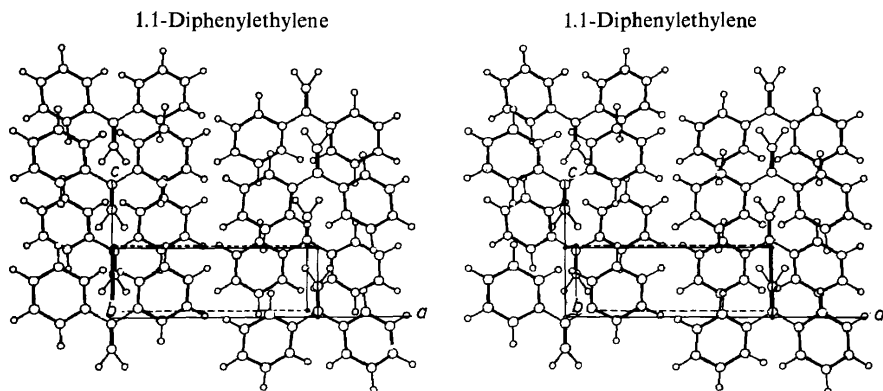


Figure 11. View of the 1,1-diphenylethylene (DPE) crystal structure.

The central 1, 2, 3, 3' C's were placed in a common plane which was the best fit plane for all the C atoms of a DPE molecule as determined by x-rays. The 2 H's on the C(1) were placed in this same best plane at the distances shown. The central C distances and angles are those given by x-ray diffraction. Three views of the DPE crystal structure, with such molecules in it, are shown in Figures 10, 11 and 12.

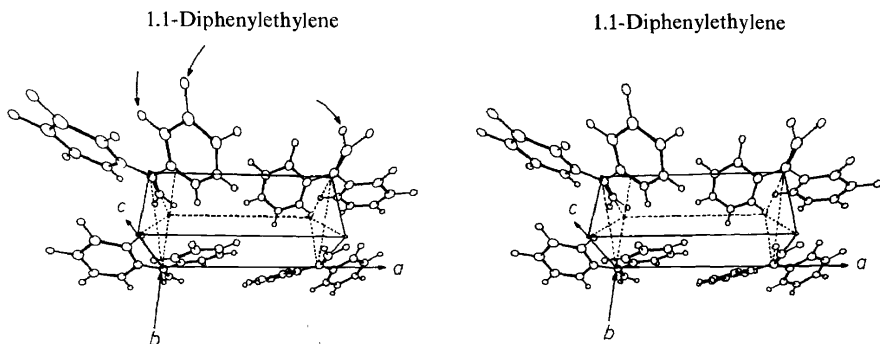


Figure 12. View of the 1,1-diphenylethylene (DPE) crystal structure.

## 7. THE LOCAL STRUCTURE AT GUEST MOLECULE SITES

In Table 11 is given a comparison of the molecular geometry of DPE determined by x-ray diffraction<sup>8</sup> and DPM geometry determined by EPR and ENDOR<sup>4,6</sup>. In this table are presented the values of the dihedral angles (closely related to the  $\phi$  angle of Figure 5) between the planes of the phenyl rings and the planes which give a least squares best fit to the coordinates of all the C atoms, the bend angle (in this table the angle given is  $2\pi - 2\theta$  in which  $\theta$  is the  $\theta$  of Figure 5), and the angle between the long axis of the molecule (which is parallel to a line through the ring centres) and the  $a$  axis of the crystal. The similarity of the values for the DPE host molecule and the DPM guest molecule is striking.

We assigned<sup>6</sup> the sets of coordinates of DPE host protons in the DPM  $x, y, z$ , axis system, obtained from the ENDOR results, to particular protons on particular host molecules as follows. Eight models of the substitution of DPM molecules into DPE sites were considered. A substituted DPM molecule may be either right handed or left handed with respect to the pitch

Table 11. Structure and orientation angles of 1,1-diphenylethylene and diphenylmethylenes in equivalent sites in 1,1-diphenylethylene crystals

	DPE	DPM
Phenyl ring twist from best molecular plane	$+0.197\pi$ ( $+35^\circ$ )	$+0.20\pi$ ( $+36^\circ$ )
Central C—C—C bond angle to rings	$0.684\pi$ ( $123^\circ$ )	$0.84\pi$ ( $151^\circ$ )
Angle between long axis and $a$ axis	$+0.019\pi$ ( $+3.5^\circ$ )	$-0.015\pi$ ( $2.8^\circ$ )

of the propellor blades formed by the phenyl rings. It may have its central C  $c$  coordinate larger or smaller than the  $c$  coordinate of the 2 C's to which it is attached. And the line of ring centres may be twisted slightly clockwise or slightly counterclockwise from the  $a$  axis looking out from the origin along the  $+c$  axis. This gives eight different kinds of orientation of the guest DPM molecule. The DPM shape determined by EPR and ENDOR was assumed. The 2-fold DPM axis was assumed to lie on the 2-fold axis of the (0,0,0) site of the DPE structure. All DPE molecules were assumed to have the *Figure 9* model structure. The coordinates of all protons of all eight DPE molecules in the nearest neighbour shell (assuming no disruption of DPE structure) about the DPM (0,0,0) site were calculated. The DPE proton coordinates previously given in *Table 10* were transformed to the crystallographic axis system, for each of the eight possible DPM orientations. For every reasonable assignment of the transformed coordinates of *Table 10* to DPE protons, the  $c$  coordinate of the DPM origin was fixed by making the average of the three measured  $c$  coordinates of DPE protons equal to the average of the three assigned proton coordinates of the model. The assignment of protons, and orientation of DPM molecules, which gave the smallest sum of the squares of the deviations of the three measured positions from the model positions was taken to be the correct assignment.

*Table 12.* Coordinates of 1,1-diphenylethylene host protons near diphenylmethylen guest molecules, from ENDOR and x-ray diffraction. (Coordinates of the protons in the crystal model are given in parentheses.)

Proton Position $k$	1(0, 0, 1)	7(0, $-\frac{1}{2}$ , $-\frac{1}{2}$ )	8(0, $-\frac{1}{2}$ , $-\frac{1}{2}$ )
$a(\text{\AA})$	+0.389 (+0.609)	+3.781 (+2.728)	+0.458 (+0.589)
$b(\text{\AA})$	+0.144 (-0.037)	-2.022 (-2.860)	-2.520 (-2.730)
$c(\text{\AA})$	+4.491 (+4.389)	-0.232 (-0.105)	-1.316 (-1.342)

In *Table 12*<sup>6</sup> are given the coordinates of these assigned protons as determined by x-rays for the simplified model of the undisturbed DPE structure and as determined by ENDOR. The coordinates in parentheses are those obtained from the model, and the others are the coordinates of the same protons obtained from ENDOR. The differences in these pairs of values may be taken to be measures of the local disruption of the DPE structure because of the presence of the DPM at that site. Of course, it was difficult to assess what part of these disagreements came from such local structure disruption and what part came from inadequacies of the DPM model.

## 8. CHEMICAL KINETICS<sup>6</sup>

### 8.1 Methods and conditions

EPR was used for quantitative studies<sup>6</sup> of the rates of (a) formation by irradiation and (b) decay of DPM in crystals of DPE containing DPDAM.

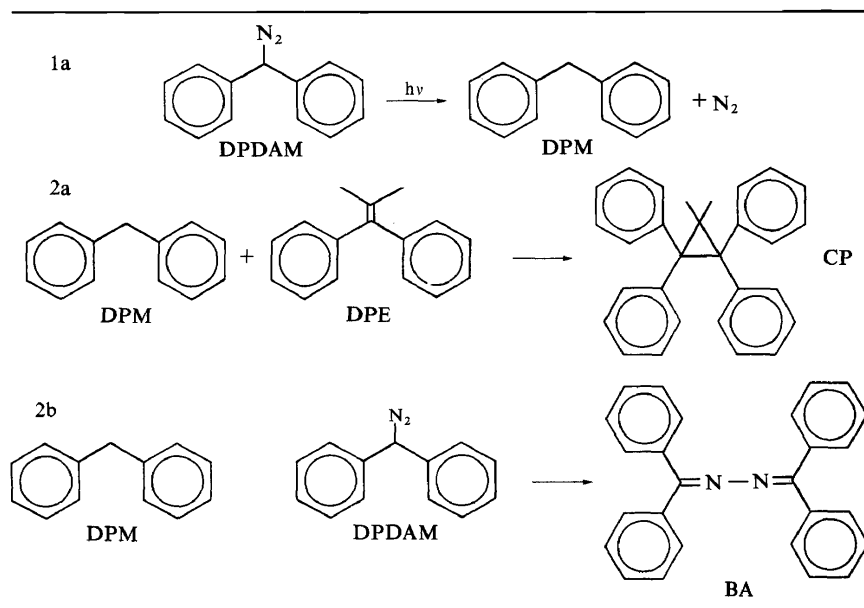
The temperature of the crystal could be controlled and measured to better than 2°K by means of thermocouples attached to the crystals during the EPR measurements. The intensity of the EPR signals was determined by means of a standard  $Mn^{+2}$  sample which was always present in the microwave cavity during the EPR measurements. The light intensity was determined by standard actinometric methods under conditions which simulated actual experiments.

Experiments were performed under a wide variety of conditions. The ranges of variables investigated are summarized in *Table 13*<sup>6</sup>.

*Table 13.* Experimental conditions for study of kinetics

1.	Light, Hg-Xe arc with 3 filters.	
1.1	UV light, ~ 2900–3200 Å	
1.2	Visible light, ~ 4800–5800 Å	
1.3	Both UV and visible	
2.	Concentration of DPDAM in DPE	
2.1	Dilute, < 0.005 mole fraction	
2.2	Concentrated, 0.023 to 0.036 mole fraction	
3.	Temperature	
3.1	Low, ~ 77°K	
3.2	High, 90–117°K	
4.	Deuteration	Code
4.1	DPDAM- $h_{10}$ in DPE- $h_2$	HH
4.2	DPDAM- $d_{10}$ in DPE- $h_2$	DH
4.3	DPDAM- $h_{10}$ in DPE- $d_2$	HD

*Table 14.* Chemical reactions.



Experiments in which large samples of DPE crystals containing DPDAM were irradiated at  $\sim 77^\circ\text{K}$ , warmed to room temperature, and analyzed by various means, showed two and only two reaction products, tetraphenylcyclopropane (CP) and benzophenone azine (BA). The only paramagnetic species ever observed under any of the experimental conditions was DPM. Thus the chemical reactions which we observed were assumed to be the three reactions described in *Table 14*<sup>6</sup>.

## 8.2 Photolysis<sup>6</sup>

Some experimentally measured values at the beginning of the irradiation, at  $\sim 77^\circ\text{K}$ , of previously unirradiated DPE crystals dilute in DPDAM are given in *Table 15*<sup>6</sup>. The spectral information for determining these values came from our optical studies<sup>7</sup> of this system.

*Table 15.* Initial experimental conditions for photolysis at the boiling point of  $\text{N}_2$ .

Light	Ultraviolet and visible	Ultraviolet	Visible
DPM production rate ( $\text{sec}^{-1}$ )	$4 \times 10^{14}$	$1 \times 10^{15}$	$2 \times 10^{12}$
Light Incidence rate ( $\text{quanta sec}^{-1}$ )	$3 \times 10^{16}$	$1 \times 10^{16}$	$7 \times 10^{16}$
Number of DPDAM's in the irradiated part of the crystal	$1 \times 10^{16}$	$3 \times 10^{15}$	$2 \times 10^{16}$
Rate of light absorption by DPDAM ( $\text{quanta sec}^{-1}$ )	$4 \times 10^{15}$	$8 \times 10^{15}$	$8 \times 10^{15}$
Fraction of quanta absorbed by DPDAM in the ultraviolet	0.13	0.54	0.00
Fraction of quanta absorbed by DPDAM in the visible	0.04	0.01	0.10

It is to be noted that the initial rate of low temperature production of DPM is much higher for ultraviolet than for visible light. This arises<sup>7</sup> partly from the fact that the DPDAM ultraviolet absorption coefficient is  $\sim 10^3 \text{ mole}^{-1} \text{ l cm}^{-1}$  and the visible absorption coefficient is  $\sim 10^2 \text{ mole}^{-1} \text{ l cm}^{-1}$ . The apparent DPM quantum yield is 0.129 in the ultraviolet and is  $1.25 \times 10^{-4}$  in the visible. We had no quantitative information on the amounts of CP formed so that some of the DPM formed could have reacted during the photolysis process to form products, in spite of the fact that when photolysis was terminated, the formed DPM was very stable.

## 8.3 Reactions of DPM<sup>6</sup>

In low concentration crystals of DPE containing DPDAM, the rate of decay of EPR signals from DPM was exponential within the errors of the measurements. In high concentration crystals, the rate of decay was the sum

of two clearly distinguishable exponential decays. In *Figure 13*<sup>6</sup> the intensity of the DPM EPR signal is plotted versus time. Curve A is for a dilute crystal at  $\sim 96^\circ\text{K}$ . Curve B is for a concentrated crystal at  $\sim 112^\circ\text{K}$ .

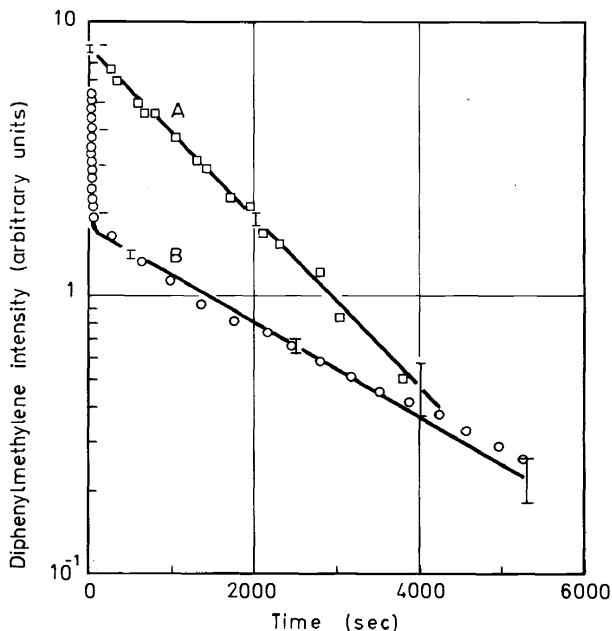


*Figure 13.* Decay of electron magnetic resonance signal from diphenylmethylene (DPM). Curve A for dilute crystal at  $\sim 96^\circ\text{K}$ . Curve B for concentrated crystal at  $\sim 112^\circ\text{K}$ .

The decays of 36 different low concentration crystals were each least squares fitted by the relation,

$$I = I_0 e^{-kt}, \quad (5)$$

in which  $I$  is the EPR signal intensity and  $t$  is time, by adjustment of the constants,  $I_0$  and  $k$ . Then the variation of the  $k$ 's, found in this manner with

*Table 16.* Values of parameters for best fit of  $\log_e(k/A) = -B/T$  to the diphenylmethylene decay in 1,1-diphenylethylene crystals. (Standard deviations are shown in parentheses).

Crystal and Decay Component	$\text{Log}_e A_n^\dagger$	$\text{Log}_{10} A_n^\dagger$	$B \times R$ kcal mole <sup>-1</sup>	$(B \times R/hc)$ (cm <sup>-1</sup> )
HH rapid decay	34 (2)	14.8	7.8 (0.3)	$2.73 \times 10^3$
DH rapid decay	28 (5)	12.2	6.7 (1.0)	$2.34 \times 10^3$
HD rapid decay	27 (2)	11.7	6.6 (0.4)	$2.31 \times 10^3$
HD slow decay	13 (3)	5.6	4.6 (0.6)	$1.61 \times 10^3$

<sup>†</sup>  $A_n$  = Numerical value of  $A$  measured in sec<sup>-1</sup>



temperature, were least squares fitted with the relation,

$$\ln(k/A) = B/T, \quad (6)$$

in which  $T$  is the temperature, by adjustment of the constants,  $A$  and  $B$ .

Plots of  $k$ 's versus  $T$ , obtained in this manner, are given in *Figure 14*<sup>6</sup> for all three isotropic systems. In *Figure 15*<sup>6</sup> are presented similar plots for

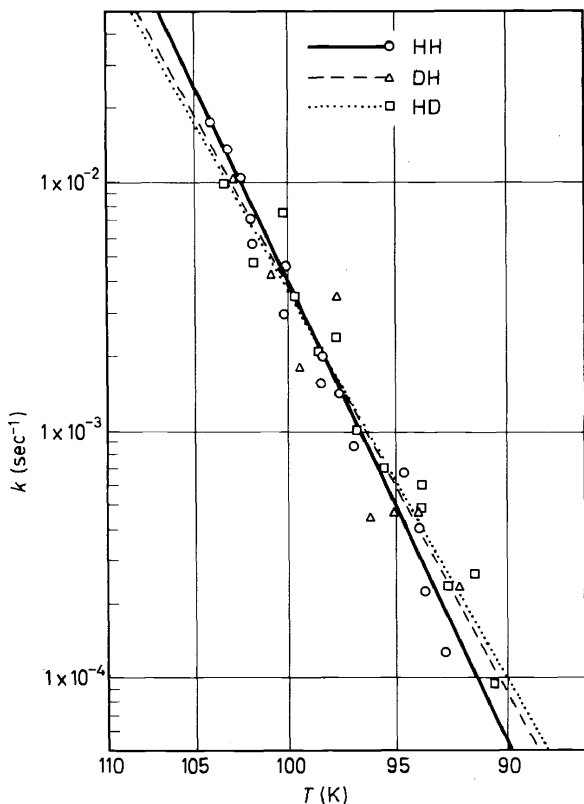


*Figure 14.*  $k$  (in (5)) vs  $T$  for the fast decay.

the slow decay process in concentrated crystals. The ratio of the  $I_0$  for the slowly decaying component to the  $I_0$  for the fast decay in the same concentrated crystal was always  $< 0.11$ .

The values of the parameters,  $A$  and  $B$ , for best fit are given in *Table 16*<sup>6</sup>.

## 9. REACTION MECHANISMS<sup>6</sup>

All of our experimental results were consistent with the occurrence of the three chemical reactions shown in *Table 14*<sup>6</sup>. We assumed that the appearance of the EPR signal is accounted for by reaction 1 and the decay by reactions 2a and 2b. We assumed that the fast decay was produced by reaction 2a and the slow decay by reaction 2b. It is important to note that the clear

distinguishability of the fast and the slow decays shows that a particular given DPM molecule must decay by a particular one of the processes, 2a or 2b; i.e. it is predestined as to which of the two decay processes is going to produce the decay of a given DPM at a given site in the crystal.

When the large crystal samples were irradiated and warmed the relative amounts of BA and CP were close to the relative values of  $I_0$ 's of (5) for the slow and the fast decay processes. This was the main reason for associating reactions 2a and 2b with CP and BA production, respectively. We thus assumed that the larger fraction of the EPR signal would decay by reaction 2a and a smaller fraction by reaction 2b.

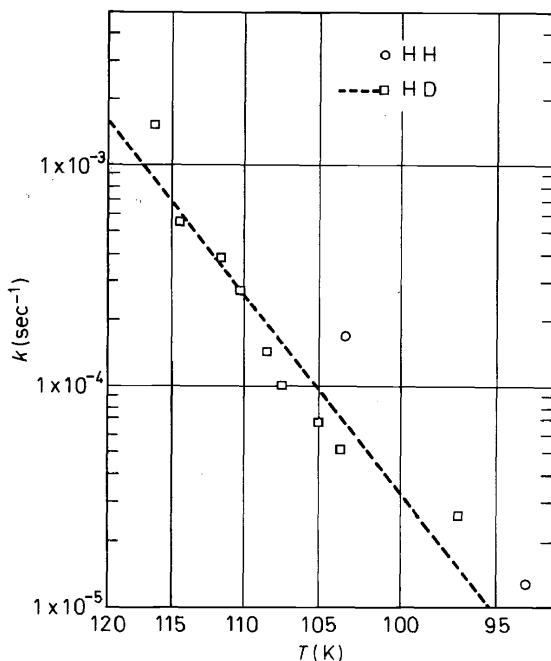


Figure 15.  $k$  (in (5)) vs  $T$  for the slow decay.

The quantum yields of DPM and the initial production rates of DPM are much larger for ultraviolet than for visible light. Our optical studies<sup>7</sup> indicated that the visible absorption of DPDAM was an  $n-\pi^*$  transition and that the ultraviolet absorption was a  $\pi-\pi^*$  transition. The C—N bond may be considerably more weakened by the  $\pi-\pi^*$  transition than by the  $n-\pi^*$  transition.

The strictly exponential decay of the DPM signal when reaction 2a occurs, and the fact that the Arrhenius type relation (6) is well obeyed, suggested to us that a thermally activated first order process was being observed<sup>6</sup>. If we interpreted the  $B$  of (6) as an activation energy, its value, which was  $\sim 7$  kcal mole<sup>-1</sup>, corresponding to  $\sim 2.45 \times 10^3$  cm<sup>-1</sup>, was certainly not nearly large enough to account for a molecular diffusion of such large molecules, if that had been the thermally activated process. It was also much too small

## EPR AND ENDOR OF REACTING TRIPLETS IN ORGANIC CRYSTALS

to account for a complete rotation of the DPE or DPM molecule in its crystal site, or a complete rotation of a phenyl ring in the DPE crystal structure. It was also clear that phase changes and crystal defects of a localized character could not be of great importance, inasmuch as the EPR spectrum showed the existence of a very high degree of molecular orientation during the reaction, and the crystals must have been highly perfect (except for the translationally coherent disordering of the structure mentioned previously). The values of  $B$  were equivalent to a few quanta of molecular vibration or to a few tens of quanta of molecule libration modes or of phonon modes.

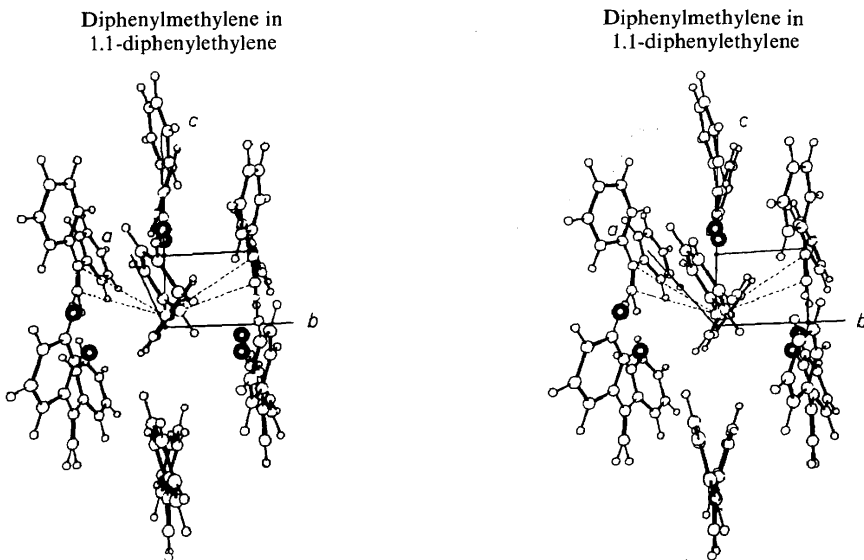


Figure 16. View of diphenylmethylene (DPM) molecule in 1,1-diphenylethylene (DPE) crystal.

We now again examine the local structure about a DPM molecules as determined from ENDOR measurements combined with the x-ray diffraction results. In Figure 16 we see a DPM molecule situated in the DPE crystal in the manner given by the ENDOR results. The three distinguishable protons whose coordinates were determined by ENDOR are represented by heavy circles. The remarkable resemblance in shapes of the DPM molecule as determined by ENDOR and of the DPE molecule as determined by x-ray diffraction is to be noted. We see, by examining this structure, that the DPE molecule which was located at the site  $(0, -\frac{1}{2}, +\frac{1}{2})$ , was ideally situated for reaction with the DPM molecule situated at the site,  $(0, 0, 0)$ . The cyclopropane ring bands that were formed are represented as broken lines in Figure 16. The plane of the cyclopropane rings that would be created, would lie nearly parallel to the  $bc$  plane. The three C atoms which would form this ring lay very close to the  $bc$  plane before reaction. The ring closure could be accomplished with only a slight movement of the pair of very bulky molecules which are involved in the chemical reaction. The distance from

the centre of the ethylene bond of the DPE molecule, at site,  $(0, -\frac{1}{2}, +\frac{1}{2})$ , to the central C atom of the DPM molecule, at site,  $(0, 0, 0)$ , was  $\sim 4.5 \text{ \AA}$ . Schmidt<sup>10</sup> has shown that two molecules, each containing ethylene bonds, will commonly react in crystals to form cyclobutane rings when the perpendicular distance between nearly parallel ethylene bonds is  $< 4.2 \text{ \AA}$ .

We proposed<sup>6</sup> that reaction 2a of *Table 14* was accomplished by a relatively very small change in the geometry and orientation of the two molecules which were involved. From data on cyclopropane bond lengths, we estimated that if the central C of the DPM moved and the two DPE C's stayed put, this central C would be required to move  $\sim 3.4 \text{ \AA}$  in order to form the CP. Of course, the actual motion distance would be expected to be less than this. It is clear that relatively low frequency vibrational modes, librational modes, and phonon modes would be involved in such a movement.

For a discussion of details of the mechanism which we have just been discussing, we chose<sup>6</sup> to consider the reaction, 2a of *Table 14*, to be a unimolecular reaction in which the reacting species was the lowest triplet state of the pair, DPE plus DPM, i.e. of the particular singlet state DPE molecule of *Figure 16* which could react with the DPM, and a DPM in its lowest triplet state, taken as a single species, with the nuclei in the positions shown in *Table 14*. The final end product was these same nuclei in their cyclopropane arrangement.

For both reactions 2a and 2b we considered two general types of mechanisms<sup>6</sup>, as follows.

(A) In one mechanism the lowest triplet state of the product lay lower in energy than populated vibrational states of the ground triplet state of the reactant.

(B) In the other mechanism, the lowest triplet state of the product lay higher in energy than any appreciably populated vibrational states of the ground triplet state of the reactant.

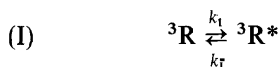
*Table 17.* Kinetic processes.

---

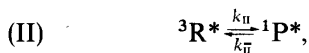
(I)	${}^3\text{R} \xrightleftharpoons[k_{\text{T}}]{k_{\text{I}}} {}^3\text{R}^*$
(II)	${}^3\text{R}^* \xrightleftharpoons[k_{\text{II}}]{k_{\text{II}}} {}^1\text{P}^*$
(III)	${}^3\text{R}^* \xrightleftharpoons[k_{\text{III}}]{k_{\text{III}}} {}^3\text{P}^*$
(IV)	${}^1\text{P}^* \xrightarrow{k_{\text{IV}}} {}^1\text{P}$
(V)	${}^3\text{P}^* \xrightarrow{k_{\text{V}}} {}^3\text{P}$
(VI)	${}^3\text{P} \xrightarrow{k_{\text{VI}}} {}^1\text{P}$

---

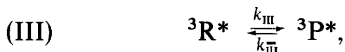
For mechanism (A) we considered<sup>6</sup> the possible processes, shown in *Table 17*;



vibrational excitation and deexcitation of the ground triplet state reactant ;



radiationless transition from the vibrationally excited triplet state of the reactant to a vibrationally excited singlet state of the product ;



radiationless transition from a vibrationally excited triplet state of the reactant to a vibrationally excited triplet state of the product ;



a vibrational deexcitation of singlet product to ground state product ;



a vibrational deexcitation of triplet state product ;



a radiationless transition from triplet state product to singlet state product followed by vibrational relaxation to ground state product.

We were never able to detect any phosphorescence arising from triplet state species during reaction, so processes such as (VI) must have been fast relative to our measured reaction rates. Processes (IV) and (V) must have also been very fast. We considered processes, (I), (II), and (III), in detail.

For the reasons about to be given we believed that the decay of DPM by reaction 2a of *Table 14* to form CP proceeded by mechanism (A) described above. Therefore processes (I), (II), and (III), needed to be considered in the discussion of the fast decay process for DPM.

In *Figure 17* we have summarized information concerning the energies of the various states of the molecules involved in reactions 2a and 2b of *Table 14*. On the left side of *Figure 17*, under A, we have given information for the reactant, DPM plus DPE, and the product, CP. Actually the solid lines are for methylene plus ethylene, as reactants, and cyclopropane as product, because sufficient experimental information on energies was not available for the phenyl substituted compounds. The consideration of the effect of substitution will be delayed for the moment. Measurements of heats of reaction have given values of the energy of ethylene plus methylene (i.e. of the reactant, R) relative to the ground state of cyclopropane<sup>11-13</sup>. This value is approximately the  $30.1 \times 10^3 \text{ cm}^{-1} \times hc$ , given as the difference between  ${}^3R$  and  ${}^1P_G$  (G stands for ground state) at the left side of A. On the other hand the best information on the difference in energy between the lowest singlet state of cyclopropane and the ground state of cyclopropane was obtained from the investigation of the thermal isomerization of cyclopropane to propylene by Chambers and Kistiakowsky<sup>14</sup>. This process was found to be a thermally activated unimolecular reaction with activation energy,

$22.7 \times 10^3 \text{ cm}^{-1} \times hc$ . There has been accumulated a very substantial amount of experimental information<sup>15, 16, 18-20</sup> related to (a) the thermal isomerization of cyclopropane to propylene, (b) the thermal *cis-trans* isomerization of deuterated cyclopropanes, and (c) the reactions of methylene with ethylene, which shows that these processes proceed via a lowest excited state of cyclopropane which resembles a trimethylene molecule. It is also clear that for such a state of cyclopropane, the singlet triplet energy difference is relatively very small<sup>17</sup>. We therefore assumed that the data of Chambers

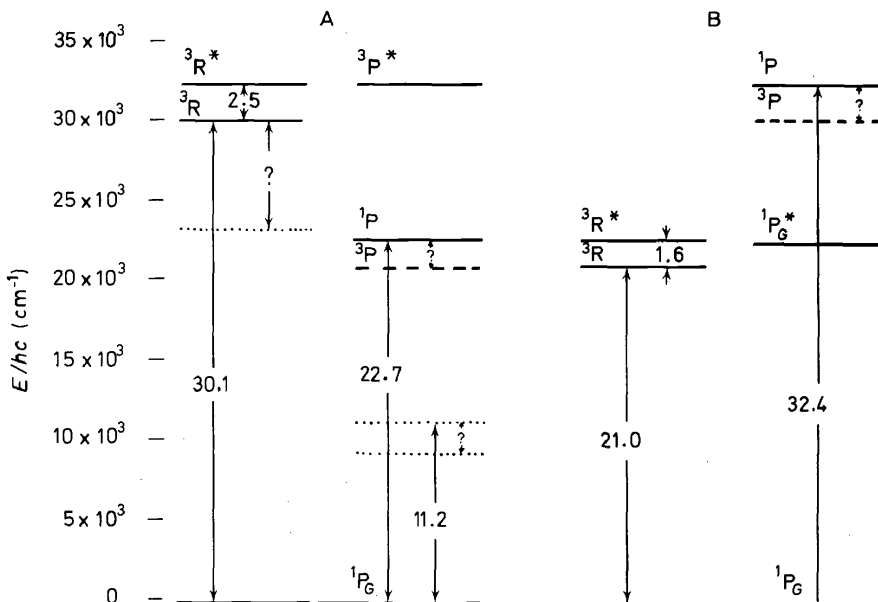


Figure 17. Energy level diagram.

and Kistiakowsky<sup>14</sup>, mentioned above, gave the difference in energy of the lowest excited and ground singlet states of the product, P, of our reaction. We arbitrarily placed the energy of the lowest triplet state of our product very close to this singlet state in energy, i.e.  $\sim 2 \times 10^3 \text{ cm}^{-1} \times hc$  lower. These levels are shown as a solid and a dashed line, respectively, on the right side of our A scheme. It is to be noted that the investigation by Schlag and Rabinovitch<sup>21</sup> of the reversible geometrical isomerization of deuterocyclopropanes showed that this reaction probably proceeded via the same excited state of cyclopropane as did the isomerization to propylene, and also had an activation energy,  $22.7 \times 10^3 \text{ cm}^{-1} \times hc$ . We thus saw that the lowest triplet state of a cyclopropane product would almost certainly be quite far, in energy, below the lowest triplet state of our reactant, triplet methylene plus ethylene. It was therefore clear that the reaction, 2a of Table 14, would be expected to proceed by general mechanism, (A). It was clear that the phenyl substitutions would have the effect of lowering the energies of the states which we have been discussing. There was no information available on phenyl substituted compounds, but Vogel and Sunderman<sup>22</sup> have

studied the thermal isomerization of *trans*-1,2-divinylcyclopropane, and they found an energy of activation,  $11.2 \times 10^3 \text{ cm}^{-1} \times hc$ . The state through which this process proceeded was undoubtedly similar to that mentioned above, and the figure just mentioned indicated that the state was lowered in energy by  $11.5 \times 10^3 \text{ cm}^{-1} \times hc$  from that of the cyclopropane, given previously. A singlet and triplet pair of levels is therefore given as a pair of dotted lines,  $11.5 \times 10^3 \text{ cm}^{-1} \times hc$  lower in energy than those of cyclopropane on the right side of the A diagram of Figure 17. The triplet state on the left side would certainly be lowered also, but by a somewhat smaller amount. We have guessed this lowering at  $\sim 7 \times 10^3 \text{ cm}^{-1} \times hc$ , and such a level is indicated on the left side of the A diagram. We thus saw that the effect of substitution would certainly leave intact our conclusion that the reaction 2a proceeded by mechanism (A).

Given that reaction 2a of Table 14 proceeds by mechanism (A) we needed to consider the processes, (I), (II), and (III), of Table 17. In view of the fact that the low frequency vibrational modes, or librational or phonon modes, were probably the active modes for the reaction, the measured values of *B* in (6) which were given in Table 16 corresponded to excitation of quite a number of such quanta, as previously mentioned. Thus the usual approximation, for unimolecular processes, of the concentration of reacting molecules as a Boltzmann factor times the concentration of ground state reactant species, with a  $\Delta E$  approximately equal to the difference in vibrational energies of the ground and reacting states of the reactant, was appropriate here. The rate of reaction was thus given by the product of this Boltzmann factor and either (a) the rate of the radiationless transition from,  $^3R^*$ , the excited triplet state of DPM + DPE, to  $^3P^*$ , a vibrationally excited triplet state of CP of the same energy, or (b) the rate of transition of  $^3R^*$  to  $^1P^*$ , an excited singlet state of CP. The observed preexponential factor, *A*, was shown in Table 16 to have a value  $\sim 10^{15} \text{ sec}^{-1}$ , for the HH system. This is just the value observed in numerous<sup>14, 21, 23, 24, 25</sup> examples of related processes, e.g. the *cis-trans* isomerizations mentioned above, in which the transition occurs between states of the same multiplicity. The radiationless transition rate, between states of different multiplicity, would be expected to be much smaller<sup>26</sup>, i.e.  $\sim 10^5 \text{ sec}^{-1}$ . Thus process (II) of Table 17 was neglected in the consideration of reaction 2a.

The foregoing reasons led us to consider that our experiments showed that reaction 2a occurred by general mechanism, (A), with vibrational excitation (process (I) in Table 17) of the ground triplet state reactant, DPM + DPE, at a particular crystal site, to a state with  $\sim 2.5 \times 10^3 \text{ cm}^{-1} \times hc$  higher energy (see *B* values in Table 16); followed by a radiationless transition (process (III) in Table 17) with frequency,  $\sim 10^{15} \text{ sec}^{-1}$  (see *A* value for HH system in Table 16), to a vibrationally excited triplet state of the product, CP, followed by rapid deexcitation of the triplet state product. The measured excitation energy,  $\sim 2.5 \times 10^3 \text{ cm}^{-1} \times hc$ , represented the vibrational excitation required in order that the Franck Condon overlap between the vibrational states of the reactant, DPM + DPE, and those of the product, CP, with appreciably different equilibrium nuclear coordinates, be sufficient to permit the radiationless transition at an appreciable rate. The product of the Boltzmann factor,  $\exp(-2.5 \times 10^3(hc/kT))$ , and the *A* value ( $\sim 10^{15}$

$\text{sec}^{-1}$ ) gave  $k$  values such as those found experimentally and plotted in *Figure 14*. The number of DPM + DPE reactant species in the crystal was typically  $\sim 1 \times 10^{15}$ . Thus at  $\sim 97^\circ\text{K}$ , process (III) was taking place at a rate of approximately  $10^{12}$  molecules  $\text{sec}^{-1}$ . A vibrational or librational state lifetime of  $\sim 10^{-11}$  sec would then give vibrational activation and deactivation rates, between the closely spaced adjacent levels of the low frequency vibrational or librational spectrum associated with the thermal activation process, which far exceed the triplet transition rate just mentioned. Thus process (III) was the rate determining process for this mode of decay of the EPR signals.

Inspection of the information contained in *Table 16* revealed that both the  $A$  value and the  $B$  value were measurably smaller for the HD system than for the HH system. If excitation of a given number of vibrational quanta of given type were required in both systems, then the deuterated system would require less energy of excitation to the extent to which the ethylenic protons play a role in the determination of the vibrational frequencies which are important in the thermal excitation. The effect of deuteration on the density of states in the R and P nuclear configurations may be such as to make this approximately the case. The reduction of the frequency of the triplet triplet transition from  $10^{14.8}$  to  $10^{11.7}$  is not surprising in view of the expected effects of deuteration on Franck Condon factors in the vibronic interaction matrix elements and on barrier transmission coefficients, both of which have a negative exponential dependence on the square roots of the nuclear masses.

Turning to a consideration of reaction 2b in *Table 14* we look at the  $B$  side of the energy level diagram in *Figure 17*. Consideration of heats of reaction similar to those which led to the figure,  $30.1 \times 10^3 \text{ cm}^{-1} \times hc$ , for the energy difference between  ${}^3\text{R}$  and  ${}^1\text{P}_G$  in the A case, lead here to the value  $21.0 \times 10^3 \text{ cm}^{-1} \times hc$ , where the reactant is DPM + DPDAM and the product is BA. On the other hand the lowest electronically excited singlet state of DPDAM which has been observed spectroscopically<sup>27</sup> is  $32.4 \times 10^3 \text{ cm}^{-1} \times hc$  above the singlet ground state, and we guessed that the triplet state would not be more than  $\sim 2 \times 10^3 \text{ cm}^{-1} hc$  below this for a molecule such as BA. This then made it clear that in the case of reaction 2b, a vibrationally excited state of the ground triplet state of the reactant which lay above it in energy by  $\sim 1.6 \times 10^3 \text{ cm}^{-1} \times hc$ , the measured  $B$  value of *Table 16*, would lie sufficiently far below the lowest triplet state of the product that no appreciably populated vibrational state of the reactant would be higher in energy than the lowest product triplet state. Thus reaction 2b was forced to go by a triplet singlet radiationless transition mechanism. In this case process (III) of *Table 17* could not occur, and the much slower spin forbidden, triplet singlet process (II) was the rate limiting process. Such spin forbidden processes were expected to occur at a frequency very much lower than the  $10^{15} \text{ sec}^{-1}$  which we have been considering; e.g. according to Cundall<sup>28</sup> they would be expected to have preexponential factors,  $\sim 10^5 \text{ sec}^{-1}$ . This is approximately what we found.

In *Figure 18* is shown a probable model of DPDAM substituted in the DPE structure. The molecule of DPAM located at the site (0, 0, +1), in the DPE structure, is in a very favourable position for reaction with the DPM molecule at the site (0, 0, 0). In *Figure 18* we have indicated, with a broken



line, the bond that was formed between the terminal N of DPDAM and the central C of DPM such that the linkage  $=C=N=N=C=$  was nearly parallel to the crystallographic  $c$  axis. If the DPDAM rings were assumed to be in the same position as the DPE rings in the equivalent site, the distance from the terminal N of DPDAM to the central C of DPM was 3.6 Å. So we believed that, just as in the case of reaction 2a, a vibrational excitation of a reactive species,  $DPM + DPDAM$ , would produce the apparently thermally activated first order process. The transition rate or preexponential factor was much smaller than for reaction 2a because process (III) of Table 17 was not possible and the much slower triplet singlet process (II) was rate determining.

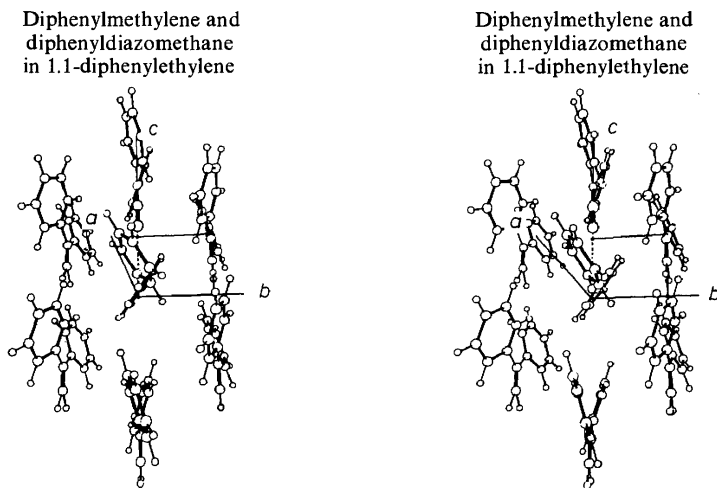


Figure 18. View of diphenyldiazomethane (DPDAM) molecule in 1,1-diphenylethylene (DPE) crystal.

It is also to be noted that the occurrence of a DPDAM molecule in such a site next to a DPM molecule must have effectively blocked the reaction of this DPM with DPE, in view of our previous remarks concerning the two distinguishable exponential decays corresponding to the two reactions, 2a and 2b of Table 14. The presence of the  $C = NN$  group apparently required prohibitively high vibrational excitation of  $DPM + DPE$  for process (III). It is, however, a matter of some surprise that such a blockage did not have an observable effect on the EPR spectrum of DPM.

#### ACKNOWLEDGEMENT

The author acknowledges the support given by the United States Atomic Energy commission for this work. Acknowledgement is also made to the donors of The Petroleum Research Fund, administered by the American Chemical Society, for partial support of this research.

Electronic equipment used in the experimental work has been supplied by the Advanced Research Projects Agency.

## REFERENCES

- <sup>1</sup> R. W. Brandon, G. L. Closs, and C. A. Hutchison Jr. *J. Chem. Phys.* **37**, 1878 (1962).
- <sup>2</sup> R. W. Brandon, G. L. Closs, C. E. Davoust, C. A. Hutchison Jr., B. E. Kohler, and R. Silbey. *J. Chem. Phys.* **43**, 2006 (1965).
- <sup>3</sup> G. L. Closs, C. A. Hutchison Jr., and B. E. Kohler. *J. Chem. Phys.* **44**, 413 (1966).
- <sup>4</sup> C. A. Hutchison Jr and B. E. Kohler. *J. Chem. Phys.* **51**, 3327 (1969).
- <sup>5</sup> C. A. Hutchison Jr. *The Triplet State*, Ed. A. B. Zahlan, page 63, Cambridge University Press, Cambridge (1967).
- <sup>6</sup> D. C. Doetschman and C. A. Hutchison Jr. Personal communication.
- <sup>7</sup> C. A. Hutchison Jr. and B. E. Kohler. Personal communication.
- <sup>8</sup> D. C. Doetschman and E. Fleischer. Personal communication.
- <sup>9</sup> E. Fleischer. Personal communication.
- <sup>10</sup> G. M. J. Schmidt. "Reactivity of the Photoexcited Organic Molecule" (*Proceedings of the 13th Conference on Chemistry at the University of Brussels*, 1965) page 227, Interscience Publishers, New York (1967).
- <sup>11</sup> H. M. Frey. Chapter 11 in *Carbene Chemistry* by W. Kirmse, page 218, Academic Press, New York and London (1964).
- <sup>12</sup> G. L. Closs. *Topics in Stereochemistry* Ed. E. L. Eliel and N. L. Allinger, page 210, Interscience Publishers, New York (1968).
- <sup>13</sup> H. M. Frey. *Progress in Reaction Kinetics* Ed. G. Porter, Volume 2, page 151, Pergamon Press, New York (1964).
- <sup>14</sup> T. S. Chambers and G. B. Kistiakowsky. *J. Am. Chem. Soc.* **56**, 399 (1934).
- <sup>15</sup> R. B. Cundall. *Progress in Reaction Kinetics* Ed. G. Porter, Volume 2, page 165, Pergamon Press, New York (1964).
- <sup>16</sup> H. M. Frey. *Advances in Physical Organic Chemistry* Ed. V. Gold, Volume 4, page 147, Academic Press London and New York (1966).
- <sup>17</sup> R. Hoffman. *J. Am. Chem. Soc.* **90**, 1475 (1968).
- <sup>18</sup> H. M. Frey. Discussion in Chapter 11, Ref. 11 above.
- <sup>19</sup> G. L. Closs. Discussion in Article. Ref. 12 above.
- <sup>20</sup> H. M. Frey. Discussion in Article, Ref. 13 above.
- <sup>21</sup> E. W. Schlag and B. S. Rabinovitch. *J. Am. Chem. Soc.* **82**, 5996 (1960).
- <sup>22</sup> E. Vogel and R. Sunderman. Referred to on page 163 of article by H. M. Frey in Ref. 16 above.
- <sup>23</sup> H. M. Frey. See Table 1, Table 2, page 152. Ref. 16 above.
- <sup>24</sup> R. J. Crawford and A. Mistra. *J. Am. Chem. Soc.* **88**, 3963 (1966).
- <sup>25</sup> J. A. Berson and J. M. Balquist. *J. Am. Chem. Soc.* **90**, 7343 (1968).
- <sup>26</sup> See for example, R. B. Cundall, page 178, Ref. 15 above.
- <sup>27</sup> E. R. Blout, V. W. Eager and R. M. Gofstein. *J. Am. Chem. Soc.* **68**, 1983 (1946).
- <sup>28</sup> R. B. Cundall. Page 178 of Ref. 15 above.
- <sup>29</sup> H. C. Longuet-Higgins and J. A. Pople. *Proc. Phys. Soc. (London)* **A68**, 591 (1955).
- <sup>30</sup> R. Pariser and R. G. Parr. *J. Chem. Phys.* **21**, 466, 767 (1953).